JCTC Journal of Chemical Theory and Computation

ARTICLE

pubs.acs.org/JCTC

Complete vs Restricted Active Space Perturbation Theory Calculation of the Cr_2 Potential Energy Surface

Fernando Ruipérez,[†] Francesco Aquilante,[‡] Jesus M. Ugalde,[†] and Ivan Infante*[,†]

[†]Kimika Fakultatea, Euskal Herriko Unibertsitatea, and Donostia International Physics Center (DIPC), P. K. 1072, 20080 Donostia, Euskadi, Spain

[‡]Department of Physical Chemistry, University of Geneva Chemical Center, 30 Quai Ernest-Ansermet, CH-1211, Geneva, Switzerland

ABSTRACT: In this paper, we calculate the potential energy surface (PES) and the spectroscopic constants of the chromium dimer using the recently developed restricted active space second-order perturbation (RASPT2) method. This approach is benchmarked against available experimental measurements and the complete active space second-order perturbation theory (CASPT2), which is nowadays established as one of the most accurate theoretical models available. Dissociation energies, vibrational frequencies, and bond distances are computed at the RASPT2 level using several reference spaces. The major advantage of the RASPT2 method is that with a limited number of configuration state functions, it can reproduce well the equilibrium bond length and the vibrational frequency of the Cr dimer. On the other hand, the PES is well described only at short distances, while at large distances, it compares very poorly with the CASPT2. The dissociation energy is also ill-behaved, but its value can be largely improved using a simple workaround that we explain in the text. In the paper, we also address the effect of the Ionization Potential Electron Affinity (IPEA) shift (a parameter introduced in the zeroth-order Hamiltonian in the CASPT2 method to include the effect of two-electron terms) and show how its default value of 0.25 is not suitable for a proper description of the PES and of the spectroscopic parameters and must be changed to a more sound value of 0.45.

1. INTRODUCTION

The interest in small transition metal (TM) clusters has grown rapidly in recent years because of their wide range of applications in different fields, such as catalysis, optics, biomedicine, environment.[1−5] TM clusters also serve as a bridge between bulk materials and nanomaterials, since they are experimentally accessible and, at the same time, still tractable with very accurate theoretical models.

From a theoretical standpoint, the description of transition metal elements and their compounds is particularly challenging due to the presence of a dense manifold of low-lying states generated by the partial occupation of the *n*d and $(n + 1)$s shells. These factors can lead to ground state (or excited state) wave functions of multireference character, where a large number of configurations is needed to properly account for *static* correlation effects, of fundamental importance for the accurate description of potential energy surfaces and dissociation energies. This precludes in many cases the use of post-Hartree−Fock methods and poses great challenges to density functional theory (DFT), as these approaches work best for the accurate description of solely the *dynamic* correlation. Under these circumstances, a multiconfigurational model such as the complete active space self-consistent field method followed by second-order perturbation theory, CASSCF/CASPT2,[6−10] is particularly attractive to achieve a proper description of both types of correlation energy.

The recent development of the so-called ab initio density fitting and Cholesky-based algorithms[11−14] has expanded considerably the range of molecular sizes for which CASSCF/CASPT2 calculations are feasible. A number of insightful studies of diverse chemical problems[15−18] has been possible as a result of these improvements in theory and algorithms. Unfortunately, the application of CASSCF/CASPT2 is still limited by the solution of the configuration interaction (CI) problem, a step where the computational cost increases factorially with the size of the active space. This adverse circumstance prevents its use for the study of TM clusters with more than two atoms. In order to overcome such limitation, new theoretical models have been introduced[19−21] to reduce drastically the number of configuration state functions (CSFs) in the CI step. In particular, the restricted active space self-consistent field method, followed by second-order perturbation theory, RASSCF/RASPT2,[19−22] is emerging as a promising alternative. Although the RASSCF method was developed 20 years ago,[19,20] its extension to include dynamical correlation, the so-called RASPT2 method,[21] was successfully established only recently. A few applications can be found already in the literature with encouraging results.[21,23−25]

To achieve the goal of studying TM clusters of increasing size, we decided to assess the performance of RASSCF/RASPT2 on a small albeit complex transition metal molecule: the chromium dimer.

The Cr_2 molecule poses a big challenge from a theoretical standpoint because its ground state presents one of the most complicated electronic structures that can be found among metal dimers. The $^1\Sigma_g^+$ electronic ground state is highly multiconfigurational, and the dominant CSF, $4s\sigma_g^2 3d\sigma_g^2 3d\pi_u^4 3d\delta_g^4$, weighs only 47% (this work). Also, the experimental potential energy surface (PES) shows, in addition to the relatively deep minimum at approximately 1.68 Å corresponding to the 3d−3d interaction, a rather flat, shelf-like region, at about 2.5 Å, where the interaction

Received: January 21, 2011
Published: April 14, 2011

between the diffuse 4s orbitals is dominant.[26] As a further complication, the dimer dissociates into two chromium atoms whose ground state has a high-spin open-shell electronic configuration ^{7}S, with six unpaired electrons distributed as $3d^5 4s^1$. This means that the static electron correlation becomes dramatically important along the potential energy surface.

Popular exchange-correlation (xc) functionals, within the framework of DFT, have been demonstrated to poorly describe the PES and some of the spectroscopic constants. Only the BLYP functional is capable of reproducing the first minimum and the shelf-like potential along the PES, while traditional hybrid functionals like B3LYP and B3PB86 fail to show the region at 2.5 Å.[27] For all xc functionals used, the stretching vibrational frequency is computed at about 800 cm^{-1}, almost 2 times larger than the experimental value, 481 cm^{-1}. Furthermore, spin contamination affects all DFT results, pinpointing the fact that a single closed-shell configuration represents a too simplistic description of the bonding pattern in the Cr dimer.

A variety of post-HF calculations have been employed to study the Cr_2 PES;[28,29] however, for the purposes of this paper, we focus on the ones based on the CASSCF/CASPT2 method. The first of these calculations showed severe problems with intruder states, and the calculations were not able to reproduce the shallow region at 2.5 Å in the potential energy surface.[30] Years later, several improvements were included in the computational model, regarding basis sets, active space, and the zeroth-order Hamiltonian. The first attempt to solve the problem of the intruder states involved the use of a modified zeroth-order Hamiltonian, called *g*1, and significant improvement was achieved. A deep inspection of the CASPT2 wave function revealed that the 4p orbitals were playing a major role in removing the intruder states; hence, the original active space, which included 12 electrons in 12 orbitals (the 3d and 4s orbitals of the two atoms), called CAS(12/12), was extended to include four extra orbitals of 4p character, more precisely the three bonding combination $4p_\sigma$ and $4p_\pi$ and the antibonding $4p^*_\sigma$. Using this big active space, it was possible to reproduce satisfactorily the shape of the potential energy surface, and the intruder-state problem was corrected applying a level shift of 0.3 au.[31]

In this work, we show that it is possible to represent correctly the spectroscopic constants and the shape of the potential energy surface for Cr_2 using the original (12/12) active space that includes the 3d and 4s orbitals, provided that an optimal value of the IPEA shift (vide infra) is chosen. Moreover, with this value of the IPEA shift, we have investigated the possibility of using the less computationally intensive RASSCF/RASPT2 method to determine the electronic structure and PES of Cr_2. Our results also provide insight into how to use the method and what its limitations are if applied to the study of bigger systems such as small metal clusters.

2. DETAILS OF THE CALCULATIONS

All-electron spin-free relativistic calculations were carried out using the Douglas−Kroll−Hess Hamiltonian.[32,33] In the first step, complete active space self-consistent field calculations (CASSCF)[6−8] are performed choosing an active space in which 12 electrons are distributed in the following 12 molecular orbitals, $4s\sigma_g$, $3d\sigma_g$, $3d\pi_u$, $3d\delta_g$, $4s\sigma^*_u$, $3d\sigma^*_u$, $3d\pi^*_g$, and $3d\delta^*_u$, composed of the 3d and 4s atomic orbitals of each Cr atom. Using this wave function, dynamical correlation effects are included through complete active space second-order perturbation theory calculations (CASPT2)[9,10] using the ionization potential electron affinity (IPEA)-corrected zeroth-order Hamiltonian[34] and the so-called *g*1 modified zeroth-order Hamiltonian.[35] The use of an imaginary shift[36] of 0.2 au was necessary in order to avoid the presence of intruder states in the CASPT2 step, where the 3s and 3p closed shells are also correlated dynamically. In the (IPEA-)corrected calculations, different values of the IPEA shift, ε, were tested. Moreover, we have also performed calculations at the RASSCF/RASPT2[19−22] level of theory, in which the zeroth-order wave function is obtained in a restricted active space (RAS). In the RASSCF method, the active space is divided into three subspaces: RAS1, RAS2, and RAS3. RAS2 is identical to the CAS, where all possible spin- and symmetry-adapted configuration state functions are constructed, i.e., a full CI within the selected space, while RAS1 and RAS3 are subspaces originally containing doubly occupied and empty orbitals, respectively. These two subspaces allow the generation of additional configuration state functions with the restriction that a maximum number of excitations may occur from RAS1 (to RAS2 and RAS3) and a maximum number of excitations may occur into RAS3 (from RAS1 and RAS2). This model can handle larger active spaces than regular CAS, provided that the resulting number of CSFs does not exceed the present limits. All calculations were performed with MOLCAS 7.4 code[37] and using C_{2h} symmetry. We used the basis set developed by Roos[31] for this system, which is obtained from the primitive basis set 21s15p10d6f4g of Pou-Amerigo et al.[38] contracted to 10s10p8d6f4g.

The potential energy surface of the Cr dimer is scanned using the VIBROT program.[37] This program fits the potential to an analytical form using cubic splines and solves the ro-vibrational Schrödinger equation numerically. The energies are then analyzed in terms of spectroscopic constants, namely, equilibrium bond length (R_e), dissociation energy (D_e and D_0), and fundamental vibrational frequency ($\Delta G_{1/2}$). The dissociation energy of the molecule can be also calculated by subtracting the ground state energy of the dimer at the equilibrium to the energy of the isolated atoms in their ground state calculated at the full CASPT2 level: $D'_e = 2 \times E[Cr(^7S)] - E[Cr_2(^1\Sigma^+_g)]$. Although this dissociation energy should be the same as the one computed with VIBROT, CASPT2 calculations lead to subtle differences due to possible numerical inconsistencies. For the sake of clarity, we show both types of dissociation throughout the paper.

The effect of counterpoise correction is minimal: 0.002 Å on the bond distance, 0.03 eV on the dissociation energy, and 10 cm^{-1} on the vibrational frequency. For this reason, we consider the BSSE noninfluential for the overall discussion, and we decided to avoid its computation for all the PESs presented in this article.

3. RESULTS

3.1. Effect of the Zeroth-Order Hamiltonian and IPEA Shift. In the original formulation of the zeroth-order Hamiltonian in the CASPT2 method, a systematic error is introduced by defining a generalized effective one-electron Fock operator that does not include explicitly two-electron terms in the Hamiltonian. In this simplified framework, a nonbalanced description of bond energies and electronic excitation energies can occur once the states that are compared have different spin-multiplicity, in particular when one of the states is a closed-shell.[39]

In order to correct this systematic error, Ghigo et al.[34] proposed a modification of the zeroth-order Hamiltonian by introducing a shift operator, the so-called Ionization Energy (IP)−Electron

Affinity (EA) shift, or more simply IPEA shift, ε, which modifies the diagonal elements of the generalized one-electron Fock matrix. Basically, in partially filled orbitals like the active orbitals in the CASSCF method, the shift modifies the diagonal elements of the Fock matrix in such a way that the energies of the active orbitals become closer to −IP, when an electron is excited out of these orbitals, and closer to −EA, when one electron is excited into one of them. This shift can be determined either using experimental results or by comparison with highly accurate calculations. For transition metals, the value of ε varies between 0.2 and 0.4 au, with an average value of 0.25 au, which is currently the default value used in the present implementation of the zeroth-order Hamiltonian in MOLCAS.[37] The addition of this parameter considerably reduces the previously mentioned systematic errors found in CASPT2 calculations; however, few studies carried out in some test cases have revealed that this is not the most appropriate value in every case.[40−42]

In this work, we study how the variation of this parameter, ε, drastically affects not only the potential energy surface but also the equilibrium bond length, the dissociation energy, and the vibrational frequency of the Cr dimer. A summary of the results is shown in Table 1 and in Figure 1.

The theoretical potential energy surface calculated using the original *g*1 zeroth-order Hamiltonian is shown in Figure 1, together with the experimental curve. It is interesting to include the *g*1 result, as it is the one based on previous calculations by Roos[31] where a bigger active space was needed together with a level shift of 0.3 au in order to accurately describe the experimental PES. In our work, for consistency with the IPEA curves, we employed an active space that includes only 3d and 4s orbitals and an imaginary level shift of 0.2 au. Under these conditions, this Hamiltonian generates a curve that agrees reasonably well with the experiment regarding the overall shape, as it reproduces the shelf-like region (see green line in Figure 1). However the first minimum, located in the 3d−3d region is much deeper than it should be and is about 0.6 eV more binding than the experimental value. Clearly, this approach is flawed since $\Delta G_{1/2}$ is also overestimated by about 100 cm^{-1} as compared to the experiment. See Table 1 for more details.

When the IPEA Hamiltonian is employed, some very interesting results are obtained. Starting with ε = 0.25, which is the default value, we notice that the shape of the curve around the 3d minimum is rather shallow, while the behavior of the curve is preserved in the 4s region (see red line in Figure 1). What is most important here is that the 3d−3d interaction is so weak that the actual bond occurs at longer distances, in the 4s−4s area. This may lead to serious errors in the geometry of the dimer, but especially in larger clusters in which the 4s interaction would always be the leading one and the clusters would show unusually large bond lengths among distinct Cr−Cr sites. To make things worse, the fundamental vibrational frequency of the Cr dimer is computed at 70 cm^{-1}, about 400 wavenumbers lower than the experimental result. It is evident from what is described above that with the default choice for the IPEA shift, we are unable to reproduce our PES, and therefore a new value of this parameter must be sought.

For ε = 0.10, the potential surface reproduces the experimental flat region, corresponding to the 4s−4s interaction; however, in the region of the 3d minimum, only a small shoulder is observed (see orange line in Figure 1). When the IPEA shift is increased to higher values, the shape of the 3d minimum is improved, while the behavior in the 4s region remains almost well-described. This means that the IPEA modifies mainly the 3d−3d interaction, while the 4s−4s is properly accounted for and rather independent from this parameter. Finally, we find that the best agreement with the experiment is achieved at a value of about ε = 0.45 (see purple line in Figure 1) where the shape of the curve reproduces accurately the region around the first minimum, both the shape and the energy, as well as the small minimum at longer distances.

Regarding bond lengths, we find that they are decreased with increasing IPEA shift, and the best agreement with the experiment corresponds to ε = 0.50 (1.681 Å calculated and 1.679 Å experimental). The *g*1 Hamiltonian also leads to satisfactory values of R_e (1.682 and 1.662 Å). The dissociation energy increases with higher values of IPEA, and the best result corresponds to ε = 0.45 (1.50 eV calculated and 1.53 eV experimental). Finally, the best agreement with experimental results for $\Delta G_{1/2}$ is obtained with ε = 0.40 (468 cm^{-1}), compared to the experimental 452 cm^{-1}.

On the basis of the above results, we decided to proceed with an IPEA shift parameter value of 0.45, which gives the best

Table 1. Spectroscopic Constants Obtained with the (IPEA-) Corrected Zeroth-Order Hamiltonian for Different Values of IPEA Shift (ε) and with the Modified *g*1 Zeroth-Order Hamiltonian[a]

ε	R_e	D_e	D'_e	D_0	$\Delta G_{1/2}$	IP
0.00			0.608			
0.25	1.736	1.15	1.38	1.14	70	7.13
0.40	1.696	1.45	1.42		468	7.12
0.45	1.687	1.52		1.50	516	7.12
0.50	1.681	1.60	1.98	1.56	542	
0.75			2.41			
1.00			2.73			
*g*1[b]	1.682	2.12	2.13	2.09	551	7.08
*g*1[c]	1.662			1.65	413	
exp.	1.679[d]	1.56		1.53[e]	452[d]	6.9988[e]

[a] The dissociation energies are calculated from the potential energy surfaces (D_e) and from 2 times the energy of the isolated atoms (D'_e). The vertical ionization potential and the experimental data are also shown. Distances in Å, vibrational frequencies in cm^{-1}, and energies in eV. [b] This work. [c] From ref 31. [d] From ref 43. [e] From ref 44.

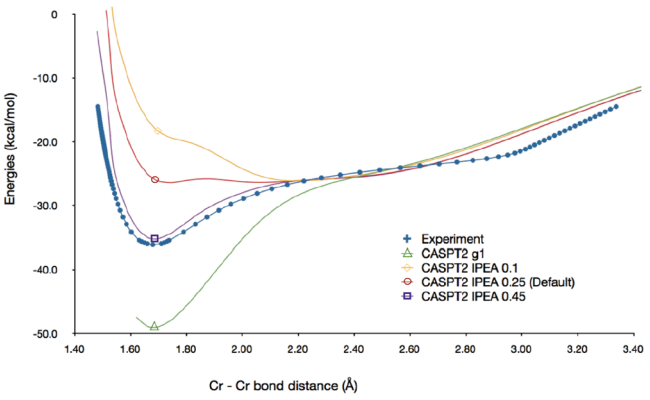

Figure 1. Potential energy surfaces obtained with different values of IPEA shift, ε, and using the modified *g*1 Hamiltonian, together with the experimental curve. Bond distances in Å and energies in kcal/mol. The asymptotic zero energy taken as reference is the total energy of the Cr atoms at a distance of 10 Å.

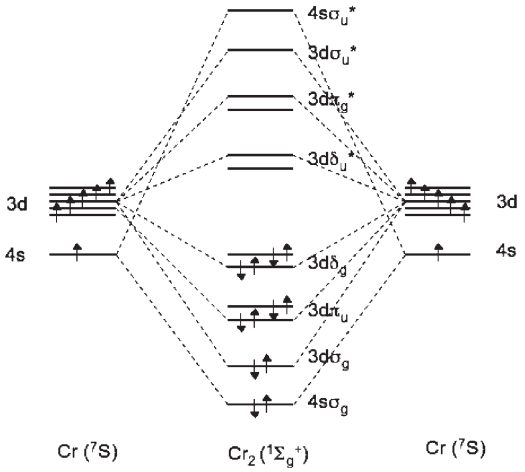

Figure 2. Schematic representation of the molecular orbital diagram for the chromium dimer. The energy ordering is arbitrary and only for didactical purposes.

compromise in terms of PES facets, dissociation energy, equilibrium bond length, and fundamental vibrational frequency.

3.2. Accuracy of Quantum Chemical Calculations: RASPT2 vs CASPT2 Results. The previous part of this work was devoted to the analysis of the effects of the IPEA shift on some properties of the chromium dimer, using high level CASSCF/CASPT2 calculations. However, as was mentioned earlier, the main goal of this paper is to benchmark the capabilities of the recently proposed RASPT2 method, which has been previously successfully employed.[21,23−25] In this part of the work, we would like to check the performance of the RASPT2 method on some properties of the Cr_2 dimer, and in order to do so, we decided to probe in a consistent way the size of the RAS subspaces (RAS1, RAS2, RAS3) with respect to the CASPT2 results.

In Figure 2, we represent a qualitative molecular orbital diagram for the dimer. This diagram will guide us in the distribution of the molecular orbitals in the different RAS subspaces. The nomenclature used in these calculations is the following: $(n_e \text{ in } n_o)/(n_{e2} \text{ in } n_{o2})//n$, where n_e in n_o is the total number of electrons distributed in the total number of orbitals in the whole active space, n_{e2} in n_{o2} corresponds to the electrons and orbitals in the RAS2 space, and, finally, n is the number of excitations allowed from RAS1 and into RAS3. The calculations performed are the following:

CAS(12/12). The CAS contains all bonding and antibonding combinations arising from the interaction of the five 3d and the 4s atomic orbitals of the two Cr atoms at the equilibrium bond length. The following molecular orbitals are obtained (Figure 2): $4s\sigma_g$, $3d\sigma_g$, $3d\pi_u$, $3d\delta_g$, $4s\sigma_u^*$, $3d\sigma_u^*$, $3d\pi_g^*$, and $3d\delta_u^*$. This level of calculation is the most accurate and will be used as a reference for RASSCF and RASPT2. In Figure 3, we immediately notice that in the CASSCF potential, the 3d−3d bond is virtually absent and is represented by a very small shoulder at about 1.80 Å . At increased distances, the energy profile becomes more stabilizing, with a large shallow minimum at about 3 Å. The facets of the PES change drastically with the inclusion of the dynamic correlation energy, thanks to the formation of a deep well in the 3d−3d bonding energy (Figure 4). This allows one to obtain the correct form of the potential, which leads to a correct description of the spectroscopic parameters in the CASPT2 results.

CAS(10/10). In this calculation, we remove from the active space the $4s\sigma_g$ bonding and $4s\sigma_u^*$ antibonding orbitals, and we

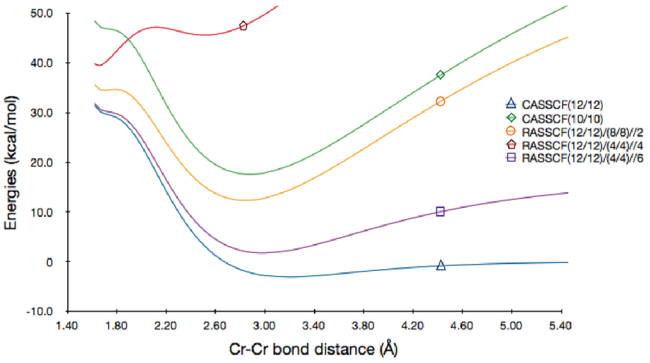

Figure 3. Potential energy surfaces calculated at CASSCF and RASSCF levels of theory. Bond distances in Å and energies in kcal/mol. For simplicity, the asymptotic zero energy taken as a reference is the total energy of the Cr atoms at a distance of 10 Å and computed at the CASSCF(12/12) level of theory. All other binding energies are depicted with respect to this value.

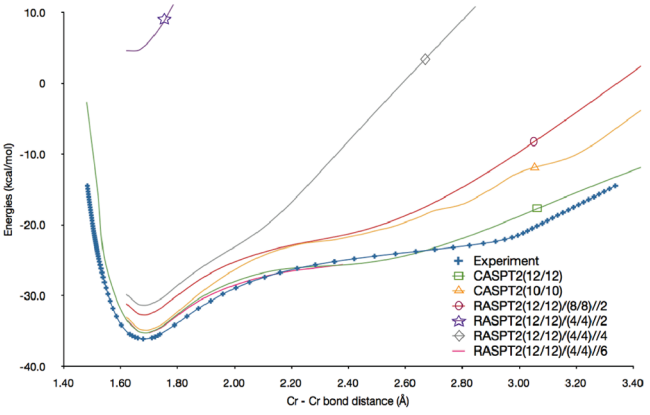

Figure 4. Potential energy surfaces calculated at different levels of theory, together with the experimental curve. Bond distances in Å and energies in kcal/mol. For simplicity, the asymptotic zero energy taken as reference here is the total energy of the Cr atoms at a distance of 10 Å and computed at the CASPT2(12/12) level of theory. All other binding energies are depicted with respect to this value. For this reason, the binding energies expressed in the figure are not equal (with the exception of the full CASPT2) to the D_e given in the tables throughout the text.

correlate them perturbatively in the CASPT2 step. This gives rise to an erratic PES for both the CASSCF and CASPT2, since the effect of the CSFs produced by excitations from (into) $4s\sigma_g$ ($4s\sigma_u^*$) is treated only perturbatively and, therefore, not accurately enough to describe the 4s−4s bond breaking. As a result, large deviations are seen in the 2.5 Å region, where the 4s−4s interaction is dominant. At short distances, the CASPT2 curve behaves accurately. The spectroscopic parameters are affected dramatically (see Table 2), with the exception of the equilibrium bond length. The dissociation energy is more binding by 2 eV, and the vibrational frequency is reduced by about 30 cm^{-1}.

RAS(12/12)/(10/10)//2. In this first RASSCF/RASPT2 calculation, the 4s bonding orbital ($4s\sigma_g$) is included in RAS1 and the corresponding antibonding ($4s\sigma_u^*$) in RAS3. Single and double excitations are allowed from $4s\sigma_g$ and into $4s\sigma_u^*$. This active space is actually equivalent to the CAS(12/12), since RAS2 produces up to 10-fold excitations that can combine with the singles and doubles from RAS1 and into RAS3, therefore reaching 12-fold

Table 2. Spectroscopic Constants and Number of Configuration State Functions (CSF) for Different Levels of Calculation Using the IPEA Shift Value $\varepsilon = 0.45$[a]

calculation	CSF	R_e	D_e	D_0	D'_e	$\Delta G_{1/2}$
CASPT2(10/10)	4956	1.689	3.40	3.37	1.10	389
CASPT2(12/12)	*57168*	*1.687*	*1.53*	*1.50*	*1.53*	*516*
RASPT2(12/12)//(10/10)//2	*57168*	*1.687*	*1.53*	*1.50*	*1.53*	*516*
RASPT2(12/12)//(8/8)//2	29244	1.682	4.26	4.23	1.41	515
RASPT2(12/12)//(8/8)//4	*57168*	*1.687*	*1.53*	*1.50*	*1.53*	*516*
RASPT2(12/12)//(4/4)//2	2298	1.641	4.17	4.15	0.30	208
RASPT2(12/12)//(4/4)//4	29164	1.681	5.94	5.90	1.35	502
RASPT2(12/12)//(4/4)//6	55126	1.687	2.33	2.30	1.53	504
RASPT2(12/12)//(4/4)//8	*57168*	*1.687*	*1.53*	*1.50*	*1.53*	*516*
RASPT2(12/12)//(0/0)//2[b]	199					
RASPT2(12/12)//(0/0)//4	7206	1.638	10.82	10.80	0.39	212
RASPT2(12/12)//(0/0)//6	37122	1.678	5.54	5.51	1.37	516
RASPT2(12/12)//(0/0)//8	55629	1.687	2.38	2.35	1.53	512
RASPT2(12/12)//(0/0)//10	57155	1.687	1.58	1.55	1.53	510
RASPT2(12/12)//(0/0)//12	*57168*	*1.687*	*1.53*	*1.50*	*1.53*	*516*
experiment		1.679		1.53		452

[a] Rows in italics denote calculations that reproduce the full CASPT2 results with the same number of CSFs. Experimental values are also included. Distances in Å, vibrational frequencies in cm^{-1}, and energies in eV. The D_e is computed following the PES from the Cr_2 ground state to the separated fragments in their ground states at the given level of theory. The D'_e is computed with respect to the isolated fragments at the full CASPT2. [b] In this RAS space, most of the calculations have diverged, and a complete description of the spectroscopic parameters is not possible.

excitations. This equivalence is obviously reflected in the number of CSFs used to build the wave function in each of the two methods, as seen in Table 2.

RAS(12/12)//(8/8)//2,4. The composition of the different spaces is as follows: RAS1($4s\sigma_g$, $3d\sigma_g$), RAS3($4s\sigma^*_u$, $3d\sigma^*_u$) and RAS2 ($3d\pi_u$, $3d\delta_g$, $3d\pi^*_g$, $3d\delta^*_u$). Basically, we exclude the most bound 3d orbital, i.e., the $3d\sigma_g$, and its antibonding counterpart from the RAS2 space. We calculated the effect of double and quadruple excitations from RAS1 and into RAS3. The latter one is equivalent to the full CASSCF/CASPT2(12/12). With the double excitations, the number of CSFs is reduced by about half, from 57 168 to 29 244. The CASPT2 PES is well described up to 2.5 Å. After this point, the curve moves upward compared to the correct behavior, and higher excitations are needed for a proper description of these long-range interactions. The RASPT2 equilibrium bond length and vibrational frequency (1.682 Å and 515 cm^{-1}, respectively) are in good agreement with the CASPT2 values (1.687 Å and 516 cm^{-1}); nevertheless, the dissociation energy is largely overestimated (4.23 eV compared to 1.50 eV). We can conclude that this level of approximation is accurate enough to describe the geometry of the dimer and the vibrational frequency, but not the dissociation energy.

RAS(12/12)(4/4)//2,4,6,8. In this calculation, RAS1 includes $4s\sigma_g$, $3d\sigma_g$, and $3d\pi_u$ orbitals; RAS3 includes $4s\sigma^*_u$, $3d\sigma^*_u$, and $3d\pi^*_g$; and finally RAS2 contains $3d\delta_g$ and $3d\delta^*_u$. Up to octuple excitations are allowed from RAS1 and into RAS3. As in the former cases, the highest order of excitations corresponds to the full CASSCF/CASPT2. For the rest, we notice some interesting things for the RASPT2 results: the number of excitations influences slightly the equilibrium bond lengths—1.641 Å for doubles, 1.681 Å for quadruples, and 1.687 Å for sextuples—and the comparison with the experiment (1.679 Å) or the CASPT2 (1.687 Å) is satisfactory. In particular, in the calculation with doubles that has only 2298 CSFs, about 20 times less than those of the full CASPT2, the geometry is reasonably well reproduced. Unfortunately, the dissociation energy is affected to a greater extent for almost all RAS spaces, showing important discrepancies with the experimental values (see Table 2). In Figure 4, it is possible to see the trends just described: in the region of the first minimum, all of the RAS spaces compare well with the experimental curve, but at longer distances, only the one including sextuple excitations shows an acceptable behavior.

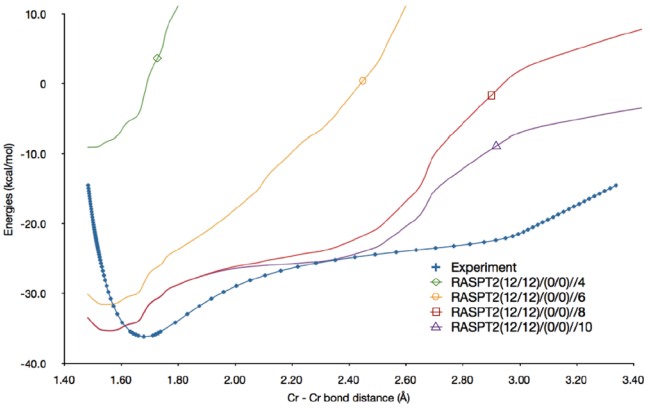

Figure 5. Potential energy surfaces calculated at RASPT2(12/12)(0/0)// 2,4,6,8,10,12 levels of theory, together with the experimental curve. Bond distances in Å and energies in kcal/mol. For simplicity, the asymptotic zero energy taken as a reference is the total energy of the Cr atoms at a distance of 10 Å and computed at the CASPT2(12/12) level of theory. All other binding energies are depicted with respect to this value. For this reason, the binding energies expressed in the figure are not equal (with the exception of the full CASPT2) to the D_e given in the tables throughout the text.

RAS(12/12)(0/0)//2,4,6,8,10,12. In this calculation, RAS1 includes the following orbitals: $4s\sigma_g$, $3d\sigma_g$, $3d\pi_u$ and $3d\delta_g$, and RAS3 includes $4s\sigma^*_u$, $3d\sigma^*_u$, $3d\pi^*_g$, and $3d\delta^*_u$ orbitals. The RAS2 subspace is empty, which means that these calculations are similar to multireference CI, except for the fact that the coefficients of the molecular orbitals are also optimized variationally. Here, we perform up to 12-ple excitations between RAS1 and into RAS3 subspaces, with this latter one corresponding to a full CASPT2(12/12). For the sake of clarity, the results are represented in Figure 5. All orders of excitations from RAS1 and into RAS3 produce reasonable results regarding equilibrium bond lengths (see Table 2); however, the dissociation energies are quite poor at first but improved notably with increasing degrees of excitation. For example, with quadruple excitations, D_e is 10.80 eV and with 10-ples is 1.55 eV, very close to the CASPT2 value (1.50 eV). The vibrational frequencies are satisfactory from sextuple excitations and up. Obviously, the best RASPT2 space is the one that includes 10-ple excitations. However, this level of calculation generates roughly the same number of configuration state functions (57155) as CASPT2 (57168), and there is no real computational advantage. A reasonable compromise is the RASPT2(12/12)(0/0)//6 space, with 37 122 CSFs, and very good equilibrium bond length and vibrational frequency are obtained.

Vibrational Levels. As a further litmus test for the RASPT2 method, we decided to compare higher vibrational levels with the

Table 3. Calculated Vibrational Frequencies[a]

v	CASA0	CASA1	CASA2	RASB//2	RASC//2	RASC//4	RASC//6	RASD//4	RASD//6	RASD//8	RASD//10	exp.
						$\Delta G_{v+1/2} = G_{v+1} - G_v$						
0	413	516	389	515	208	502	504	212	516	512	510	452
1	439	477	140	436	171	442	443	178	452	452	450	423
2	428	431	130	371	156	382	381	161	396	391	391	405
3	401	373	146	336	148	340	326	150	356	338	340	365
4	370	322	153	300	144	313	284	142	320	297	299	340
5	335	281	156	270	140	289	250	136	296	265	266	315
6	298	244	159	243	137	271	222	131	280	237	236	280
7	259	204	161	221	133	258	198	128	264	214	208	250
8	218	151	162	201	130	249	173	125	254	192	176	210
MUE	22	38	160	33	186	25	45	186	23	36	37	
						$G_{v+1} - G_o$						
0	413	516	389	515	208	502	504	212	516	512	510	452
1	852	993	529	951	379	944	947	390	968	964	960	875 ± 10
2	1279	1424	659	1322	535	1326	1328	551	1364	1355	1351	1280 ± 10
3	1681	1797	805	1658	683	1666	1654	701	1720	1693	1691	1645 ± 10
4	2050	2119	958	1958	827	1979	1938	843	2040	1990	1990	1985 ± 15
5	2385	2400	1114	2228	967	2268	2188	979	2336	2255	2256	2300 ± 15
6	2683	2644	1273	2471	1104	2539	2410	1110	2616	2492	2492	2580 ± 20
7	2942	2848	1434	2692	1237	2797	2608	1238	2880	2700	2700	2830 ± 20
8	3160	2999	1596	2893	1367	3046	2781	1363	3134	2876	2876	3040 ± 20
MUE	65	93	914	76	1076	34	110	1067	65	75	77	

[a] Nomenclature: CAS and RAS stand for CASPT2 and RASPT2, respectively. A1 and A2 stand for active spaces of types (12/12) and (10/10). A0 results are taken from ref 31. B for (12/12)/(8/8). C for (12/12)/(4/4), and D for (12/12)/(0/0). Experimental data are taken from ref 26. Mean unsigned error (MUE) is given in the last row.

available experimental values, from $v = 0$ to $v = 8$, for $\Delta G_{v+1/2}$ and $G_{v+1} - G_0$.[26] In Table 3, we report a summary of all the results. The last row identifies the mean unsigned error, MUE. The first eye-catching feature is that the previous results by Roos carry an overall error lower than the present calculations, including our full CASPT2. This is probably due to the fact that to describe with even more accuracy the upper vibrational levels, we would need to include the 4p orbitals in the active space. Moreover, apart from the RAS spaces with the lowest number of excitations (in the table, referred to as A2, C//2, and D//4), we obtain a satisfactory agreement between the RASPT2 values and the experiment, with MUE varying between 23 and 45 cm^{-1} for $\Delta G_{v+1/2}$ and between 34 and 77 cm^{-1} for $G_{v+1} - G_0$. It is noteworthy that cancellation of errors makes some of the RASPT2 active spaces more accurate than the full CASPT2.

3.3. Discussion and Conclusions. The RASPT2 method carries limited advantages over CASPT2 in the specific case of the Cr dimer. The best compromise of accuracy vs computational advantage is obtained by RASPT2(12/12)/(8/8)//2, which describes quite well the equilibrium bond length and the vibrational frequency. Unfortunately, the dissociation energy is somewhat off, as it is in most of the RAS spaces we have chosen. To fix this problem and to get more accurate values for the dissociation, we then decided to make use of a simple workaround. Instead of taking the atoms at large distances and computing the energy with the same RAS space used at the equilibrium, we used the energy of the isolated atoms computed at the full CASPT2 level of theory. This energy is cheap to calculate because the atom has a reduced active space, i.e., (6/6), and a full CASPT2 accounts for only a small number of CSFs. If we take this CASPT2 energy as a reference for the atomic fragments, the RASPT2 dissociation energies are improved. In Table 2, they are represented with the acronym D'_e. The maximum error is contained within about 1.2 eV, while already with some higher order of excitations from RAS1 and into RAS3, this error can be contained within the 0.2−0.3 eV. It is evident that the improvement is huge, as the error is drastically reduced by a factor of 3 to 5. This way of proceeding, however, introduced an imbalance between the active space used for the atomic fragments and that for the dimer at the equilibrium. This imbalance holds at the CASSCF (or RASSCF) step, but it is virtually canceled out at the PT2 level, when also the 3s and 3p orbitals are perturbatively correlated using all virtual orbitals, restoring in this way a numerical size consistency.

In conclusion, if one would like to study a cluster with more Cr atoms, it is wise to proceed with a balanced RASPT2 space, not necessarily too big, to obtain reasonable geometries and frequencies. For the dissociation energy, as explained above, it is always better to take the fragments computed with the most accurate method available, keeping the size consistency at the PT2 step.

We must also consider that in this paper we have chosen to benchmark an extremely complicated molecule that shows a heavy multiconfigurational character and a complicated potential energy surface. This had repercussions, as we have seen, not only on the RASPT2 method but also on the IPEA shift, which we had to tune to a value of 0.45 for a correct description of the potential energy surface and the spectroscopic constants. It may be interesting to apply the RASPT2 method and check the default value of the IPEA shift for other transition metal dimers, where these limitations can be less pronounced and where RASPT2

may show significant computational advantages over CASPT2, contrary to what observed for the Cr dimer.

Overall, RASPT2 appears as a computationally viable alternative to CASPT2 for studying stationary points on a PES, but it may fail to reproduce some details of the surface, as shown by the peculiar case of Cr_2.

AUTHOR INFORMATION

Corresponding Author

*Fax: +34-943-015270. E-mail: iinfant76@gmail.com.

ACKNOWLEDGMENT

Financial support comes from Eusko Jaurlaritza and the Spanish Office for Scientific Research. The SGI/IZO-SGIker UPV/EHU is gratefully acknowledged for generous allocation of computational resources. I.I. would like to thank the Spanish Ministry of Science and Innovation for a Juan de la Cierva fellowship.

REFERENCES

(1) Baletto, F.; Ferrando, R. *Rev. Mod. Phys.* **2005**, *77*, 371.
(2) Barden, C. J.; Rienstra-Kiracofe, J. C.; Schaefer, H. F. *Chem. Rev.* **2000**, *100*, 637.
(3) Morse, M. D. *Chem. Rev.* **1986**, *86*, 1049.
(4) Caada-Vilalta, C.; O'Brien, T. A.; Brechin, E. K.; Pink, M.; Davidson, E. R.; Christou, G. *Inorg. Chem.* **2004**, *43*, 5505.
(5) Gutsev, G. L.; Bauschlicher, C. W., Jr. *J. Phys. Chem. A* **2003**, *107*, 7013.
(6) Roos, B. O.; Taylor, P. R.; Siegbahn, P. E. M. *Chem. Phys.* **1980**, *48*, 157.
(7) Siegbahn, P. E. M.; Heiberg, A.; Roos, B. O.; Levy, B. *Phys. Scr.* **1980**, *21*, 323.
(8) Siegbahn, P. E. M.; Heiberg, A.; Almlöf, J.; Roos, B. O. *J. Chem. Phys.* **1981**, *74*, 2384.
(9) Andersson, K.; Malmqvist, P.-Å.; Roos, B. O.; Sadlej, A. J.; Wolinski, K. *J. Phys. Chem.* **1990**, *94*, 5483.
(10) Andersson, K.; Malmqvist, P.-Å.; Roos, B. O. *J. Chem. Phys.* **1992**, *96*, 1218.
(11) Pedersen, T. B.; Aquilante, F.; Lindh, R. *Theor. Chem. Acc.* **2009**, *124*, 1.
(12) Aquilante, F.; Todorova, T.; Pedersen, T. B.; Gagliardi, L.; Roos, B. O. *J. Chem. Phys.* **2009**, *131*, 34113.
(13) Aquilante, F.; Pedersen, T. B.; de Meras, A. S.; Koch, H. *J. Chem. Phys.* **2008**, *129*, 24113.
(14) Aquilante, F.; Malmqvist, P.-Å.; Pedersen, T. B.; Ghosh, A.; Roos, B. O. *J. Chem. Theory Comput.* **2008**, *4*, 694.
(15) Srnec, M.; Aquilante, F.; Ryde, U.; Rulisek, L. *J. Phys. Chem. B* **2009**, *113*, 6074.
(16) Huber, S. M.; Ertem, M. Z.; Aquilante, F.; Gagliardi, L.; Tolman, W. B.; Cramer, C. J. *Chem.—Eur. J.* **2009**, *15*, 4886.
(17) La Macchia, G.; Li Manni, G.; Todorova, T. K.; Brynda, M.; Aquilante, F.; Roos, B. O.; Gagliardi, L. *Inorg. Chem.* **2010**, *49*, 5216.
(18) Sala, X.; Ertem, M. Z.; Vigara, L.; Todorova, T. K.; Chen, W.; Rocha, R. C.; Aquilante, F.; Cramer, C. J.; Gagliardi, L.; Llobet, A. *Angew. Chem., Int. Ed.* **2010**, *49*, 7745.
(19) Olsen, J.; Roos, B. O.; Jørgenssen, P.; Jensen, H. J. A. *J. Chem. Phys.* **1988**, *89*, 2185.
(20) Malmqvist, P.-Å.; Rendell, A.; Roos, B. O. *J. Phys. Chem.* **1990**, *94*, 5477.
(21) Malmqvist, P.-Å.; Pierloot, K.; Shahi, A. R. M.; Cramer, C. J.; Gagliardi, L. *J. Chem. Phys.* **2008**, *128*, 204109.
(22) Li Manni, G.; Aquilante, F.; Gagliardi, L. *J. Chem. Phys.* **2011**, *134*, 034114.
(23) Shahi, A. R. M.; Cramer, C. J.; Gagliardi, L. *Phys. Chem. Chem. Phys.* **2009**, *11*, 10964.
(24) Infante, I.; Kovacs, A.; La Macchia, G.; Shahi, A. R. M.; Gibson, J. K.; Gagliardi, L. *J. Phys. Chem. A* **2010**, *114*, 6007.
(25) Sauri, V.; Serrano-Andrés, L.; Shahi, A. R. M.; Gagliardi, L. *Phys. Chem. Chem. Phys.* **2009**, *11*, 10964.
(26) Casey, S. M.; Leopold, D. G. *J. Phys. Chem.* **1993**, *97*, 816.
(27) Bauschlicher, C. W., Jr.; Partridge, H. *Chem. Phys. Lett.* **1994**, *231*, 277.
(28) Muller, T. *J. Phys. Chem. A* **2009**, *113*, 12729.
(29) Celani, P.; Stoll, H.; Werner, H. J.; Knowles, P. *J. Mol. Phys.* **2004**, *102*, 2369.
(30) Andersson, K.; Roos, B. O.; Malmqvist, P.-Å.; Widmark, P.-O. *Chem. Phys. Lett.* **1994**, *230*, 391.
(31) Roos, B. O. *Collect. Czech. Chem. Commun.* **2003**, *68*, 265.
(32) Douglas, M.; Kroll, N. M. *Ann. Phys. (N.Y.)* **1974**, *82*, 89.
(33) Hess, B. A. *Phys. Rev. A* **1986**, *33*, 3742.
(34) Ghigo, G.; Roos, B. O.; Malmqvist, P.-Å. *Chem. Phys. Lett.* **2004**, *396*, 142.
(35) Andersson, K. *Theor. Chim. Acta* **1995**, *91*, 31.
(36) Forsberg, N.; Malmqvist, P.-Å. *Chem. Phys. Lett.* **1997**, *274*, 196.
(37) Aquilante, F.; De Vico, L.; Ferré, N.; Ghigo, G.; Malmqvist, P.-Å.; Neogrády, P.; Pedersen, T. B.; Pitonak, M.; Reiher, M.; Roos, B. O.; Serrano-Andrés, L.; Urban, M.; Veryazov, V.; Lindh, R. *J. Comput. Chem.* **2010**, *31*, 224.
(38) Pou-Amerigo, R.; Merchán, M.; Widmark, P.-O.; Roos, B. O. *Theor. Chim. Acta* **1995**, *92*, 149.
(39) Andersson, K.; Roos, B. O. *Int. J. Quantum Chem.* **1993**, *45*, 591.
(40) Queralt, N.; Taratiel, D.; de Graaf, C.; Caballol, R.; Cimiraglia, R.; Angeli, C. *J. Comput. Chem.* **2008**, *29*, 994.
(41) Suaud, N.; Bonet, M.-L.; Boilleau, C.; Labèguerie, P.; Guihéry, N. *J. Am. Chem. Soc.* **2009**, *131*, 715.
(42) Kepenikian, M.; Robert, V.; Le Guennic, B. *J. Chem. Phys.* **2009**, *131*, 114702.
(43) Bondybey, V. E.; English, J. H. *Chem. Phys. Lett.* **1983**, *94*, 443.
(44) Simard, B.; Lebeault-Dorget, M. A.; Marijinissen, A.; ter Meulen, J. J. *J. Chem. Phys.* **1998**, *108*, 9668.